Available online at www.sciencedirect.com

ScienceDirect

Ceramics International 40 (2014) 5635–5643

CERAMICS INTERNATIONAL

www.elsevier.com/locate/ceramint

Improved properties of hydroxyapatite–carbon nanotube biocomposite: Mechanical, in vitro bioactivity and biological studies

Susmita Mukherjee[a,*], Biswanath Kundu[b,**], Swarnendu Sen[c], Abhijit Chanda[d]

[a]School of Materials Science and Nanotechnology, Jadavpur University, Kolkata 700032, India
[b]Bioceramics and Coating Division, CSIR-Central Glass and Ceramic Research Institute, Kolkata 700032, India
[c]Department of Mechanical Engineering, Jadavpur University, Kolkata 700032, India
[d]School of Bioscience and Engineering, Jadavpur University, Kolkata 700032, India

Received 2 October 2013; received in revised form 30 October 2013; accepted 31 October 2013
Available online 12 November 2013

Abstract

The present work describes a simple shear mixing technique for developing a hydroxyapatite (HAp)–carbon nanotube (CNT) nanocomposite and the effect of reinforcement on the physical, mechanical, in vitro bioactivity and biological properties of HAp. XRD and FTIR confirmed that the main phase of the composites is HAp. HRTEM images demonstrated the formation of a two-dimensional nanocomposite structure, whereas FESEM images indicated the formation of nanosized HAp grains featuring sporadically distributed CNT molecules. No major phase changes in HAp were observed with up to 5% added CNT. However, adding more than 1% CNTs caused an increase in internal crystal strain and increased substitution of CO_3^{2-} for OH^- and PO_4^{3-} groups in pure HAp. The average crystallite size increased from ~46 nm to ~100 nm with only 0.5% added CNT, remained nearly unaffected up to 2% CNTs thereafter and suddenly decreased at 5% CNTs (~61 nm). The FESEM and HRTEM images clearly showed the attachment of MWCNT chains on HAp grains, which directly affected the samples' fracture toughness and flexural strength. Of the samples, 1% showed maximum values of K_{1C}, whereas 5% showed maximum values of HV and three-point bending flexural strength. The in vitro bioactivity indicated increased apatite formation on the sample surface up to 1% CNTs after 24 weeks. However, adding 2% and 5% CNTs resulted in a manifold increase in apatite formation up to 12 weeks, after which dissolution increased up to 24 weeks, possibly due to increased substitution of CO_3^{2-} for OH^- and PO_4^{3-} groups. This result is confirmed by the FTIR studies. For all added CNT contents, all samples exhibited high haemocompatibility. However, there was a compromise between the observed mechanical properties and in vitro bioactivity studied up to 24 weeks, and care must be taken before selecting any final application of the nanocomposites.

Keywords: Hydroxyapatite; Carbon nanotube; In vitro bioactivity; Fracture toughness; Haemocompatibility

1. Introduction

Since the discovery of carbon nanotubes by Ijima [1], CNTs have emerged as a prospective candidate for materials research due to their special structural features and excellent properties, such as their extremely small dimensions, high aspect ratio (10^3–10^4) and low density, in addition to high tensile strength (~60 GPa), high rigidity (Young's modulus ~1 TPa), high resilience, superb flexibility and excellent electrical ($>105\ Sm^{-1}$) and thermal properties [2–4]. Therefore, CNTs are primarily being used as a reinforcement material in the preparation of nanocomposites, which is expected to produce composites with improved mechanical properties compared to those of single-phase materials. Ruoff et al. determined that when an advancing crack with sufficient stress intensity at its tip encounters multiwalled carbon nanotube (MWCNT) chains, the concentric layers collapse and absorb the associated energy, arresting the propagation of the crack [5]. This mechanism was identified as a toughening mechanism in CNT-based composites. Lupo et al. successfully fabricated ZrO_2/CNT composites by hydrothermal crystallisation [6], and Seeger et al. synthesised MWCNT/SiO_2 composites via partial matrix melting with a Nd:YAG laser [7].

Hydroxyapatite (HAp) has been exclusively used as a bone implant material due to the similarity between its chemical

*Corresponding author. Tel.: +91 9674459006.
**Corresponding author. Tel.: +91 9831772081.
E-mail addresses: susm08@gmail.com (S. Mukherjee), biswa_kundu@rediffmail.com, biswa.kundun@gmail.com (B. Kundu).

0272-8842/$ - see front matter © 2013 Elsevier Ltd and Techna Group S.r.l. All rights reserved.
http://dx.doi.org/10.1016/j.ceramint.2013.10.158

composition and crystal structure and that of the inorganic component of bone [8] as well as its excellent ability to bond with living bone tissues. However, the intrinsic brittleness and poor mechanical properties of sintered HAp restricts its employment in major load-bearing applications. Pure HAp has been reported to have low toughness (0.8–1.2 MPa $m^{1/2}$) and poor flexural strength (< 140 MPa) compared to human bone [8]. Therefore, HAp is being predominantly used either as a coating material on various implant materials, such as steel, titanium and titanium alloys [9], or as a scaffold for tissue engineering [10]. To improve the mechanical properties of HAp without sacrificing its biological properties, different reinforcing phases, such as zirconia, glass, silver, carbon fibre, alumina and TiO_2, have been used [11–14]. Some advanced processing techniques (e.g., high pressure and microwave sintering [15]) have also been investigated recently. Researchers are also using carbon nanotubes or nanofibres (CNT/CNF) as a reinforcing material in the HAp matrix to improve its mechanical properties [16–18]. Different techniques, such as the sol–gel process [17], laser surface alloying [19], spark plasma sintering [9] and high-precision plasma spraying [9], have been used to prepare HAp–CNT composites.

Most of the above-mentioned processes require the functionalisation of ceramics, which further requires the use of precision techniques. In the present work, we adopted an alternative and cost-effective shear mixing technique to prepare CNT–HAp composites with different proportions of pristine CNT molecules and investigated the effect of the reinforcement on the physical, mechanical, biological and in vitro bioactivity properties of HAp. The CNT–HAp composites were prepared by adding different weight percentages of CNT, and a comparative analysis of the various properties is reported.

2. Experimental

2.1. Materials

Analytical grade ortho-phosphoric acid (H_3PO_4) and calcium hydroxide ($Ca(OH)_2$) (S.D. Fine-Chem Ltd., India) were used as starting reagents for the synthesis of pure hydroxyapatite (HAp) powder via the wet chemical method. The detailed methods used for this synthesis and characterisation have been described elsewhere [20]. MWCNTs (> 95% purity, 10–30-nm diameter and 1–10 μm average length) were procured from Nanoshel LLC, USA.

2.2. HAp–CNT composite preparation

Calcined (800 °C) HAp and CNT powders (with four different CNT contents of 0.5%, 1%, 2% and 5%) were mixed counterclockwise in a high-energy planetary ball mill (Fritsche Pulverissette 5, Germany) at 300 rpm for 5 h in acetone. To minimise contamination during milling, a zirconia pot and balls with a ball-to-powder weight ratio of 10:1 were used. The milled powders were sieved and used to prepare pellet samples (12 mm diameter × 4 mm thick) in a uniaxial press (PEECO, India) at 150 MPa for 2 min. Sintering was performed in two steps in argon. In the first step, the temperature was increased to 700 °C at a heating rate of 3 °C/min. Then, the temperature was increased to 1250 °C at a heating rate of 6 °C/min (1 h dwelling at the highest temperature).

2.3. Characterisation

The apparent porosity (A.P.) and bulk density (B.D.) of the sintered specimens were estimated by Archimedes' water displacement method using the formulae [B.D. $= D/(W-S)$ g/cm^3] and [A.P. $= (W-D)/(W-S)100\%$], where D is the dry weight, W is the soaked weight and S is the suspended weight, and the relative density was calculated from the theoretical density.

X-ray diffraction (XRD, Ultima III Rigaku, Japan) and Fourier transform infrared spectroscopy in the mid-IR range (FTIR, IR Prestige 21, 200VCE, Schimadzu, Japan) were used to characterise the prepared phases. The microstructure and morphology of the nanocomposites were studied using field emission scanning electron microscopy (FESEM, Hitachi, S4800, Japan) and high-resolution transmission electron microscopy (HRTEM, JEOL, JEM 2100, Japan).

The hardness and fracture toughness (K_{1C}) of the polished sintered samples (< 0.02 μm R_a) were evaluated using an automated Vickers hardness testing machine (LECO, LV-700AT, MI) via the indentation method (ASTM C1327). Four different indentation loads of 0.3, 1, 3 and 5 kg were applied to each sample with a holding time of 10 s. A minimum of six measurements were obtained for each sample, and the average was used to calculate VH. K_{1C} was calculated using the equation for a radial-median crack: $K_{1C} = 0.016(E/H)^{0.5}(P/C^{1.5})$, where E is Young's modulus (obtained from the nano-indentation method, not discussed here), H is the Vickers hardness, P is the indentation load and C is the half-radial crack length. This equation was used because the c/a value was greater than 2.5, where c is the average crack length and a is the average crack diagonal [21,22].

The flexural strength of the nanocomposites was evaluated using a universal testing machine (Instron 4204) by three-point bending following ASTM C1674, and fractography images were obtained using an FESEM. For the flexural strength measurements, bar samples were prepared, cold-isostatically pressed at 150 MPa and sintered under an argon atmosphere at 1250 °C. The flexural strength was calculated by using the equation $\sigma = 3Fl/2bd^2$, where l is the specimen length, F (N) is the total force applied to the specimen by the loading pin and b and d are the specimen width and thickness, respectively.

The haemocompatibility of the nanocomposite samples was tested with the samples in contact with mammalian blood to verify their cytotoxicity for their use in biomedical implants (following the guidelines of ASTM F756 specifications), where the physiological tolerance of the implant material was evaluated by calculating the % haemolysis in blood. In this process, goat blood, which was pre-treated with sodium citrate (anti-coagulant), was collected and diluted with normal saline to a ratio of 8:10. The samples, which were in the form of round pellets (with no sharp edges), were placed in standard

test tubes containing 10 mL of saline and incubated at 37 °C for 30 min to allow thermal equilibration. Then, 0.2 mL of the diluted blood was added to the sample test tubes, mixed gently and incubated at 37 °C for 60 min. A positive control was prepared by adding 10 mL of a 1% Na_2CO_3 solution (Na_2CO_3 causes large scale rupture of RBC) to 0.2 mL of the diluted blood, and for the negative control, saline (it does not rupture RBC) was used instead of Na_2CO_3. Both the positive and negative controls were incubated at 37 °C for 60 min to allow thermal equilibration. After the incubation period, the sample test tubes as well as the positive and negative controls were centrifuged for 5 min (RCF 500*g*). The supernatant was collected, and the *OD* was measured at 545 nm using a UV spectroscopic method. The % haemolysis is calculated based on the following equation:

$$\%Haemolysis = \frac{OD(test) - OD(negative)}{OD(positive) - OD(negative)}$$

The in vitro bioactivity of the composites was investigated by immersing disc specimens in simulated body fluid (SBF) prepared in the laboratory according to the protocol previously reported by Kokubo [23]. Appropriate quantities of the reagents, including NaCl, $NaHCO_3$, KCl, $K_2HPO_4 \cdot 3H_2O$, $MgCl_2 \cdot 6H_2O$, $CaCl_2$, Na_2SO_4 and Tris buffer, were dissolved in 1 L of de-ionised water under constant stirring to ensure complete dissolution. Dilute HCl was added to maintain the pH at 7.4 ± 0.1 at 37 °C. The compositions of the SBF used in the present study are provided in Table 1. A set of two samples for each composition was immersed in 15 mL of a freshly prepared SBF solution under static conditions in an incubator at pH 7.4 and 37 °C and studied for up to 24 weeks. To avoid saturation, SBF was replaced with freshly prepared solution every three days. At the end of the 2nd, 4th, 8th, 12th and 24th week, the samples were removed, dried at 65 °C and weighed. The surface morphology and microstructures of the samples were observed using an SEM, and changes in the composition on the top surface with time were measured using FTIR.

3. Results and discussions

3.1. Physical properties

The changes in the A.P., B.D. and relative density have been plotted as a function of the CNT content in Fig. 1. Upon the addition of the CNTs, the B.D. first increased up to 1% CNT, then decreased up to 5% CNT, and the opposite trend was observed for A.P. The open porosity was determined to be ~19% for the 5% CNT samples. Because the density of CNTs is substantially less than that of HAp, the addition of CNTs reduces the overall density of the composite. However, the density of 2% samples was similar to the density of pure HAp.

Table 1
Approximate composition of SBF used in the study [23].

Ionic concentration (mmol/dm^3)	SBF	Blood plasma
Na^+	142.0	142.0
K^+	5.0	5.0
Mg^{2+}	1.5	1.5
Ca^{2+}	2.5	2.5
Cl^-	147.8	103.0
HCO_3^-	4.2	27.0
HPO_4^-	1.0	1.0
SO_4^-	0.5	0.5

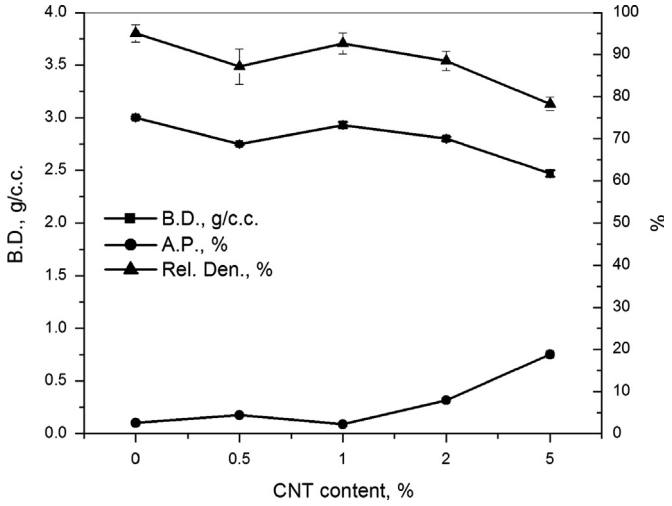

Fig. 1. Variations in A.P., B.D. and relative density as a function of % CNT. The theoretical density of HAp was 3.16 g/cm^3.

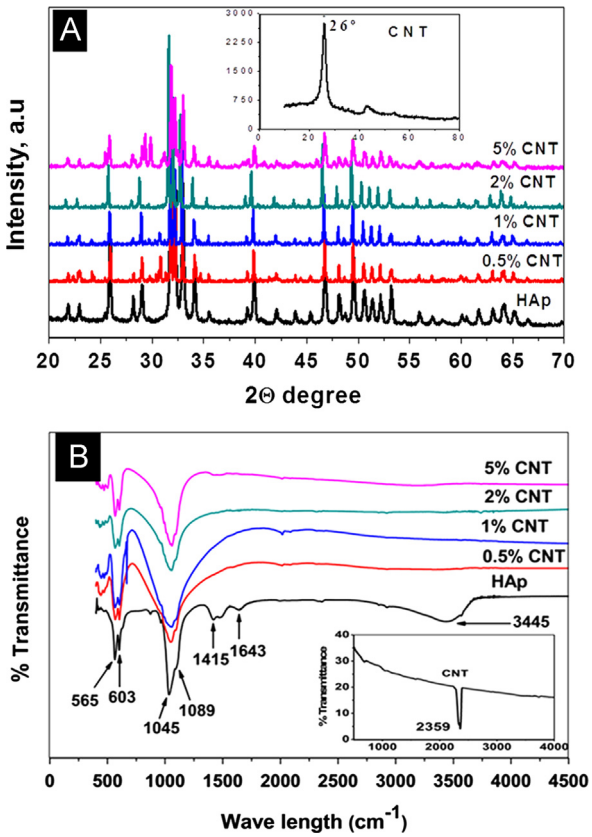

Fig. 2. (A) XRD patterns and (B) FTIR spectra of HAp and HAp–CNT composites with the pattern of the pure CNTs shown in the inset.

3.2. XRD analysis and microstructure

Fig. 2A shows the XRD pattern of the HAp–CNT composites, with the inset showing that of pure CNT. No new peaks were observed in the XRD pattern due to the addition of different CNT amounts, and the 2θ values are in agreement with those of pure HAp (JCPDS no. 09-432). The average crystallite size (τ) was calculated from the XRD plots using the Scherrer equation [24]: $\tau = K\lambda/\beta \cos\theta$, where K is a constant (shape-factor) whose value is 0.9, λ is the wavelength of the X-ray line used and β (in rad) is the full width at half-maximum (FWHM). To investigate whether the presence of CNTs in the composite resulted in any internal strain within the samples, the William–Hall and Scherrer methods were applied. The resulting internal strain, ε, was calculated using the Williamson–Hall equation [24]: $\beta \cos\theta = K\lambda/\tau + 4\varepsilon \sin\theta$, where θ is the diffraction angle, β is the FWHM at θ and ε is the mean inhomogeneous strain. A graph of $\beta \cos\theta$ and $\sin\theta$ was plotted, and the internal strain was calculated from the slope of the graph. τ and the calculated internal strain were plotted with variation in the CNT content, as shown in Fig. 3.

τ is the average grain size for the sintered samples. As indicated in Fig. 3, the grain size drastically increased from 46 nm to 100 nm when 0.5% CNTs were added to pure HAp and remained constant up to 2% CNT. The CNTs facilitated rapid grain growth up to 2% CNT addition, with concomitant crystal strain [25]. At 5% CNT addition, the grain size decreased to 61 nm, with very high crystal strain. Grain coarsening was most likely predominant when more than 2% CNTs were added to pure HAp, with an increased porosity and decreased density.

The results of the XRD analysis were correlated with those shown in Fig. 4, which shows the FESEM microstructure of pure HAp and the HAp–CNT composites. The images show fine hair-like CNT molecules (shown with arrows) attached to the HAp grains. The nanocomposites were observed to possess a porous microstructure, which is highly favourable for cellular growth. For the composite containing 5% CNTs, the CNT chains were observed to occur in an agglomerated state (in bundles) along the boundaries of the HAp grains. Based on the micrographs, the adopted fabrication method does not ensure the uniform dispersion of CNTs. In fact, agglomerates were often formed and the average particle size increased sporadically with no relationship to the addition of CNTs.

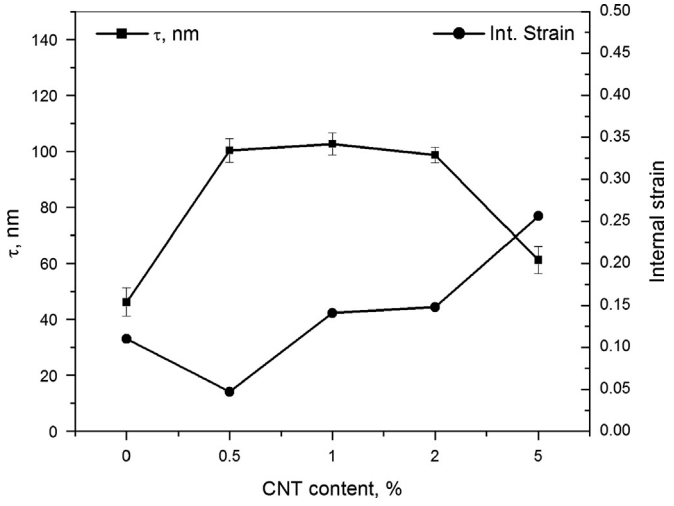

Fig. 3. Variations in the average crystallite size and internal strain with % CNT.

The microstructure of HAp–CNT nanocomposite powders was studied using HRTEM, and the results are shown in Fig. 5 before (A) and after sintering (B). The green powder (Fig. 5A) shows distinct HAp particulates with an average size of 100–150 nm attached to the CNT molecules. After sintering, agglomerates of CNTs were formed, and a multi-layered sheet-like structure was obtained, in which the HAp particles adhered to CNT layers.

3.3. FTIR analysis

The FTIR spectra of the various CNT reinforced HAp are shown in Fig. 2B, and the FTIR spectra of the pristine MWCNTs are shown in the inset. The pristine CNT spectrum exhibits a single peak at 2359 cm^{-1}, which is quite similar to that reported in the literature [26]. Pure HAp exhibits FTIR peaks at 565, 603, 1045, 1089, 1415 (attributed to the PO_4^{3-} group), 1643 and 3445 cm^{-1} (corresponding to the OH^- group). The composites exhibit peaks similar to those of pure HAp, except for those of the hydroxyl group (3OH), which is due to the loss of extra moisture during the sintering process. Therefore, the presence of CNTs in the composites does not change the basic structure of HAp. The absence of any new peaks confirms that no primary bonds formed and that the association between HAp and CNT is purely physical.

3.4. Mechanical properties

Fig. 6 shows the microhardness and K_{1C} of the nanocomposites with increasing CNT content. The hardness of the composites varied between 2.5 and 3.5 GPa (within experimental scatter). From the plots, K_{1C} of different HAp–CNT composites was observed to vary between 1.0 and 1.9 MPa $m^{1/2}$ in contrast to the value of 0.87 MPa $m^{1/2}$ observed for pure HAp, and the maximum value was observed for 1% CNT content. The plot shows that the incorporation of 1% CNTs into the HAp matrix provided a two-fold improvement in toughness due to the energy absorbed by the MWCNT chains with the collapse of concentric C-layers when subjected to external stress, in agreement with the results reported by Ruoff and Lorents [5]. This energy absorption mechanism favours the dissipation of energy, which enhances the toughness of the HAp composite. The carbon nanotubes most likely provided obstructions or ligaments to enhance the fracture energy. Human bone typically produces K_{1C} values between 2 and 4 MPa $m^{1/2}$ depending on the age of the person [27], and in the current study, the 1% CNT composite achieved a toughness value similar to that of human bone. HV increased from 3.2 to 3.4 GPa when 0.5% CNTs were added to the pure HAp matrix. However, further CNT addition up to the content of 2% degraded the HV values (2.5 GPa), and better values (3.4 GPa) were observed when 5% CNTs were added. This result indicates that the hardness values were slightly affected by

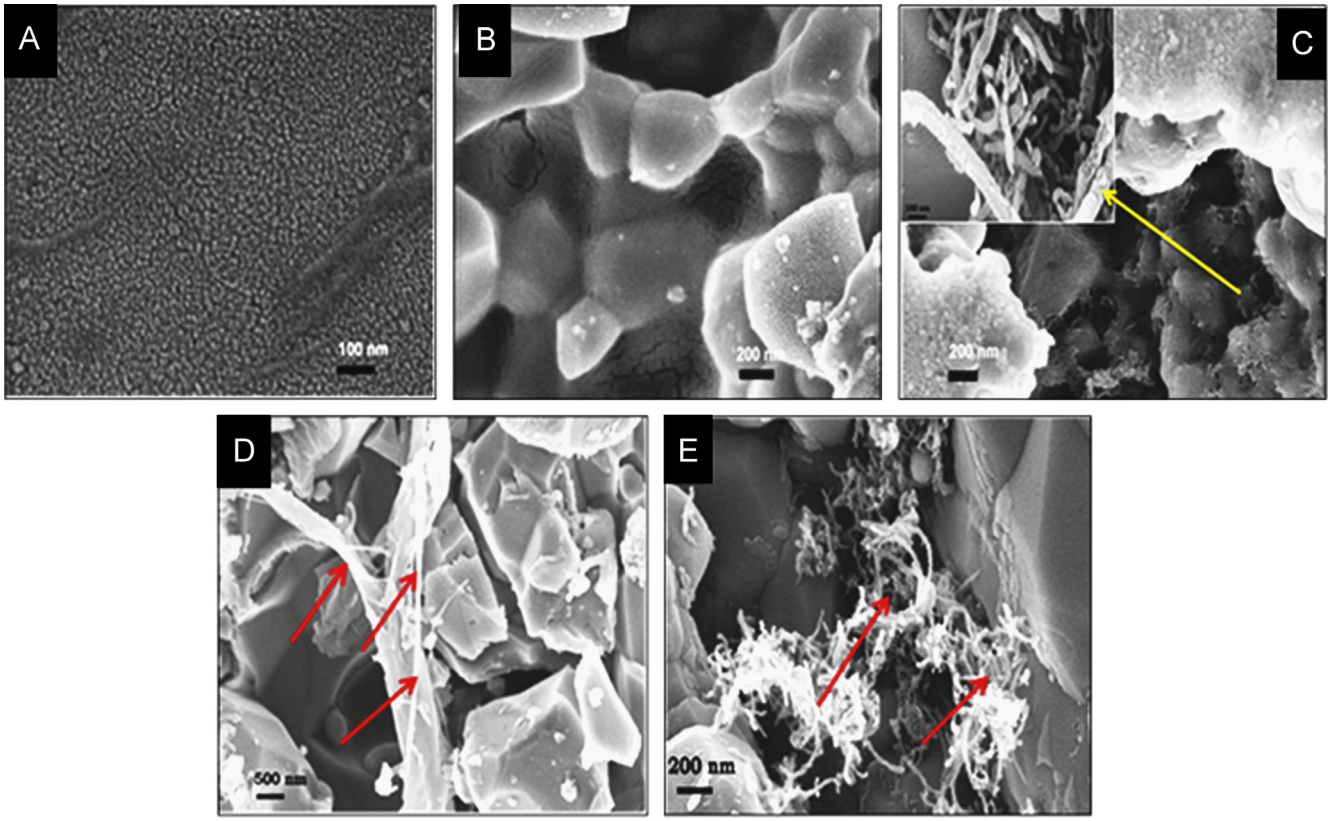

Fig. 4. Photomicrographs (FESEM) of the sintered HAp–CNT composites with various CNT contents [(A) 0%, (B) 0.5%, (C) 1%, (D) 2% and (E) 5%].

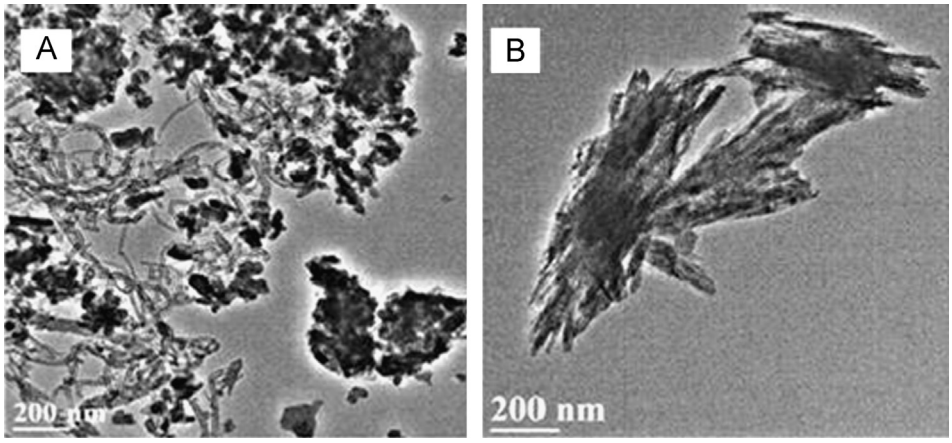

Fig. 5. HRTEM images of the HAp–CNT powders (A) before sintering and (B) after sintering.

a small addition of CNTs to pure HAp. However, further addition of CNTs was detrimental to this property primarily due to the CNT's effect on the formation of pores at the sintering temperature.

Fig. 7 shows the % increase in the flexural strength of the composites compared to that of pure HAp. The nanocomposites with a 1% and 2% CNT content exhibited a 95–120% increase, whereas the nanocomposite with a 5% CNT content exhibited an approximately 175% increase in the flexural strength over that of pure HAp. In a three-point bend test, the concave face of a sample undergoes maximum compressive stress while the other face (convex face) experiences maximum tensile stress. The flexural strength is the maximum tensile stress value that can be sustained before the sample fails, and most materials fail under tensile stress before they fail under compressive stress [28]. Based on the results shown in Fig. 7, the flexural strength demonstrated a manifold improvement with the addition of more than 0.5% CNTs due to the CNT's superior tensile properties being imparted to the nanocomposite.

Fig. 8 shows an FESEM image of the fractured surface of a pure HAp sample (Fig. 8A) and that of the 1% HAp–CNT composite sample (Fig. 8B). Fig. 8B clearly shows a CNT chain acting as a bridge across a crack moving along the boundaries of the HAp grains, confirming the anticipated hindrance of intergranular crack propagation due to the presence of ligaments. In pure HAp, the bridging action was

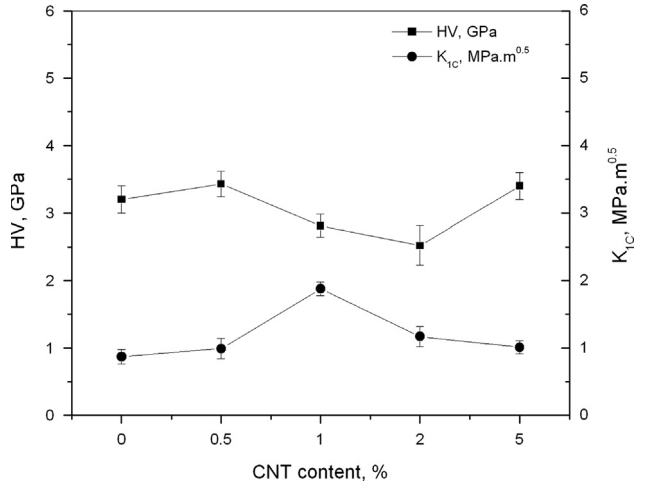

Fig. 6. Variations in HV and K_{1C} with the addition of CNTs to the HAp matrix.

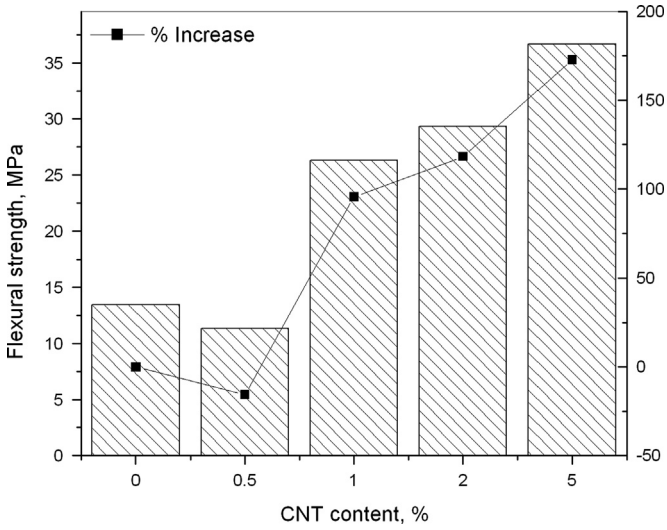

Fig. 7. Percent increase in the flexural strength (after three-point bend test) with the addition of CNTs to the HAp–CNT nanocomposites.

not observed in the corresponding fractograph (Fig. 8A). This result is in agreement with the higher K_{1C} and flexural strength values observed after the addition of 1% CNTs.

3.5. Bioactivity study

Apatite growth was determined to be the lowest after two weeks for each nanocomposite composition and the highest for samples containing up to 1% CNTs after 24 weeks, as shown in Figs. 9 and 10. However, the 2% and 5% CNT composites exhibited rapid apatite dissolution after 12 weeks and up to 24 weeks. In these samples, apatite formation was the highest at 12 weeks, which was also observed in the SEM microstructure [Fig. 9A, D and G for pure HAp, Fig. 9B, E and H for 1% CNT nanocomposite samples and Fig. 9C, F and I for 2% CNT-nanocomposite samples after being maintained in SBF for 0, 4 and 12 weeks, respectively]. Based on the results presented in Figs. 9 and 10, the CNTs added to the pure HAp matrix improved the bioactivity of the nanocomposites. Due to dissolution and deposition phenomena during the initial stages, apatite formation was observed to be the lowest after two weeks, which slightly improved after four weeks (cf. Fig. 9D–F). The deposition of apatite crystals was predominant and reached its highest level for the 5% CNT samples after 12 weeks (cf. Fig. 9G–I). Pores in the nanocomposite microstructure could be observed on the 0th day (prior to SBF immersion) (cf. Fig. 9A–C). The composition of the apatite layer grown on the samples' surface over time was studied by FTIR, and the results are shown in Fig. 11. As the number of days in the SBF increased, the substitution of CO_3^{2-} for the OH^- and PO_4^{3-} groups of HAp increased, reaching its maximum extent for the 2% and 5% CNT samples. The increased dissolution of apatite observed at 24 weeks for these two types of samples was due to the replacement of PO_4^{3-} groups inside the crystal structure of HAp. Because the PO_4^{3-} groups provide the structural stability of HAp [29], the loss of this group after 12 weeks results in faster dissolution. The conversion of crystalline HAp to more CO_3^{2-}-substituted HAp over time (in SBF) was enhanced when more CNTs were added to the composite, and this effect was observed to be the greatest after the addition of 1% CNTs in the absence of structural OH^-. Additionally, the very high crystal strain of both 2% and 5% CNT samples (0.148 and 0.256, respectively), indicating a potentially higher free energy, promoted faster dissolution after 12 weeks.

Cellular tests confirmed that carbon nanotubes offer good biocompatibility [30,31]. Zanello et al. [32] demonstrated that bone cells can grow, generate apatite granules as extracellular materials and multiply on a CNT scaffold, which makes it an ideal candidate for bone engineering. The observations made in the current study confirm these results.

3.6. Haemocompatibility study

Haemolysis is a measure of cytotoxicity of a biomaterial towards red blood cells (RBCs). Cytotoxicity results in the rupture of RBC membranes and the release of haemoglobin. Spectrometry of the free haemoglobin allows the estimation of the extent of cytotoxicity. The results obtained from haemocompatibility tests are shown in Table 2. The % haemolysis was determined to vary between 0.3 and 5.3. As per the ASTM standard, if the % haemolysis of any material is less than 10%, it is considered to be haemocompatible, and if it is less than 5%, it is highly haemocompatible. Therefore, the HAp–CNT composites are haemocompatible. In addition, HAp and the HAp–CNT composites did not physically damage the blood cells, in contrast to the positive control. The haemocompatibility of CNTs is often the subject of scrutiny due to potential metallic impurities, such as Ni. The results obtained in this study clearly demonstrate that the HAp–CNT composites exhibit very good haemocompatibility.

No major phase changes in HAp were observed upon the addition of up to 5% CNTs. However, when more than 1% CNTs were added, an increase in the internal crystal strain and increased substitution of CO_3^{2-} for the OH^- and PO_4^{3-} groups of pure HAp

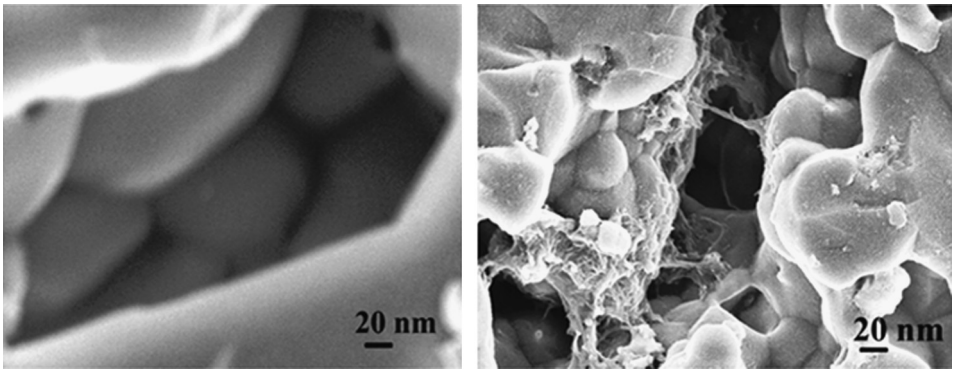

Fig. 8. FESEM images of the fractured surface of pure HAp and the 1% CNT–HAp nanocomposite.

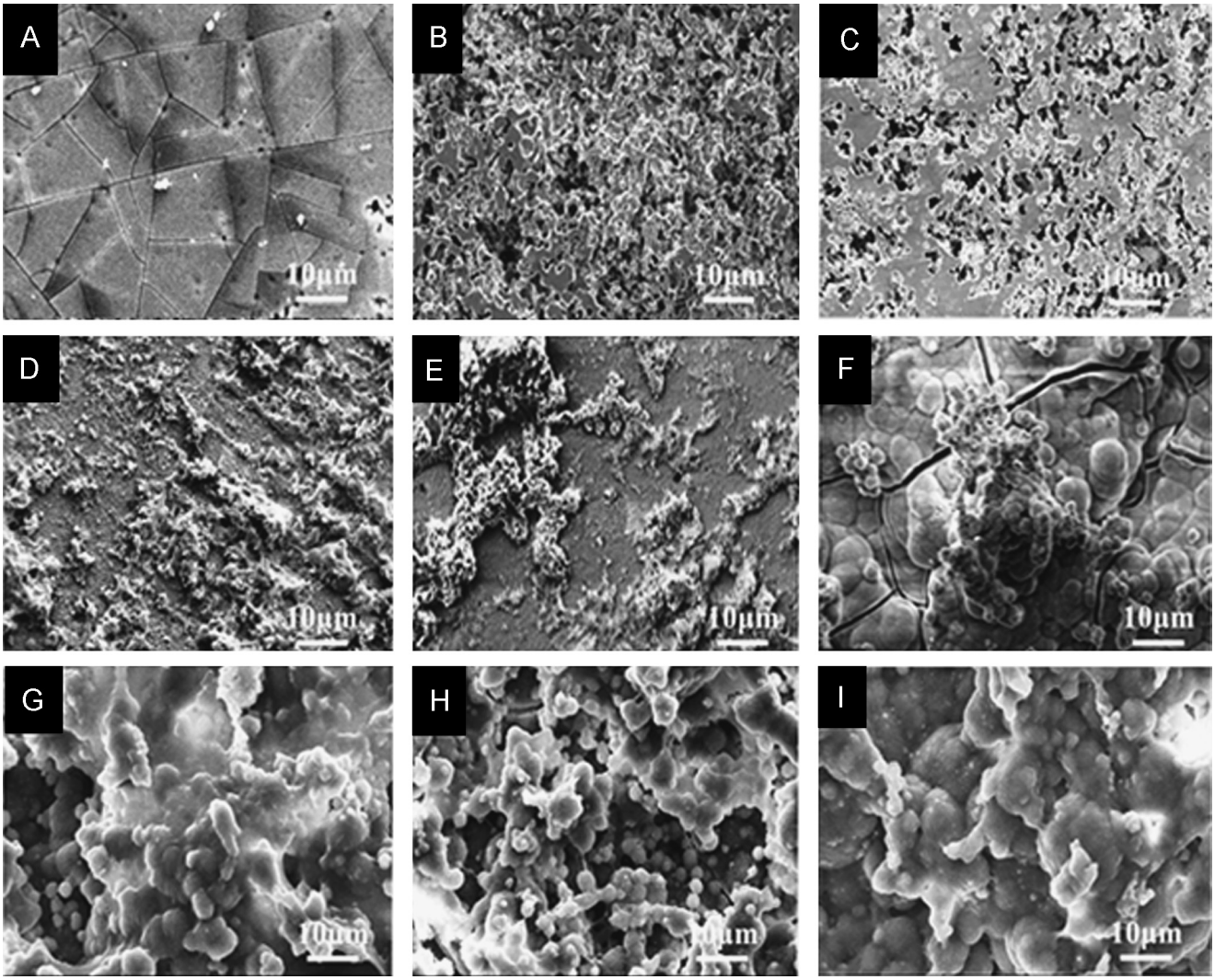

Fig. 9. Apatite formation at 0th, 4th and 12th week for pure HAp (A, D and G), 1% HAp–CNT nanocomposite (B, E and H) and 2% HAp–CNT nanocomposite (C, F and I).

were observed. The average crystallite size increased from ~46 nm to ~100 nm with the addition of 0.5% CNTs. This crystallite size was maintained up to a CNT content of 2%, and a sudden decrease in the crystallite size was observed at a CNT content of 5% (~61 nm). The microstructure observed by FESEM and HRTEM clearly indicated the attachment of MWCNT chains to the HAp grains, which directly affected K_{1C} and flexural strength of the samples. The 1% CNT samples exhibited maximum K_{1C} values, and the 5% CNT samples exhibited maximum values for HV and three-point bending flexural strength. The in vitro

bioactivity indicated increased apatite formation on the sample surface up to 1% CNTs after 24 weeks, whereas the samples containing 2% and 5% CNTs exhibited a manifold increase in apatite formation up to 12 weeks. After 12 weeks, increased dissolution was observed up to 24 weeks, which was most likely due to the increased substitution of CO_3^{2-} for the OH^- and PO_4^{3-} groups. This result was confirmed by FTIR studies. All of the samples were determined to be highly haemocompatible.

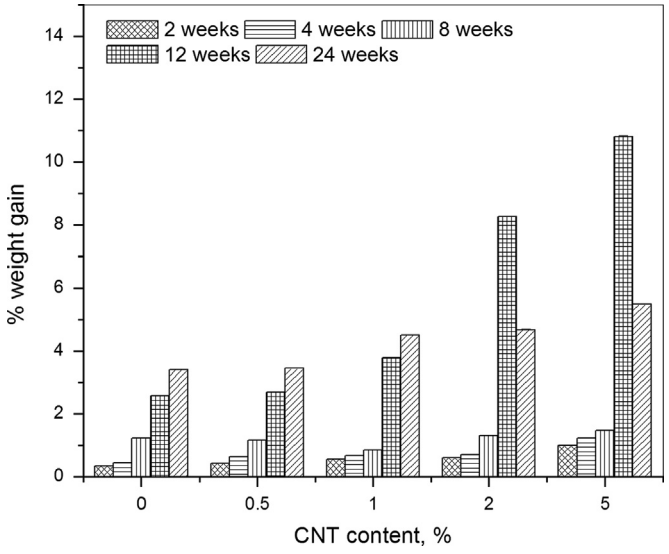

Fig. 10. % Weight gain of nanocomposite samples as a function of the time immersed in SBF for the bioactivity study.

4. Conclusion

We observed that pure HAp can be reinforced with pure CNTs using a simple shear mixing technique. We studied the physical, mechanical and biological properties of pure HAp and samples containing various CNT contents (i.e., 0.5–5%). The composites containing 5% CNTs primarily contained uniformly distributed nanosized particles and exhibited good density and approximately 19% porosity. The CNT molecules form agglomerates along the grain boundaries of HAp. These agglomerates can form bridges across advancing cracks and thus retard crack propagation. The 1% CNT–HAp composite, which showed 2% porosity and 2.93 g/c.c. B.D., exhibited a substantial improvement in toughness (120%) without significantly compromising its hardness (2.8 GPa) and flexural strength (26 MPa). The sample also exhibited lower internal crystal strain (0.14) and an average crystallite size of 102 nm. This nanocomposite also exhibited substantially enhanced

Table 2
Haemolysis (%) of HAp–CNT composite samples.

Sample	% Haemolysis
HAp	0.343
HAp–CNT (0.5%)	0.958
HAp–CNT (1%)	1.150
HAp–CNT (2%)	1.753
HAp–CNT (5%)	2.853
Positive control	100
Negative control	0

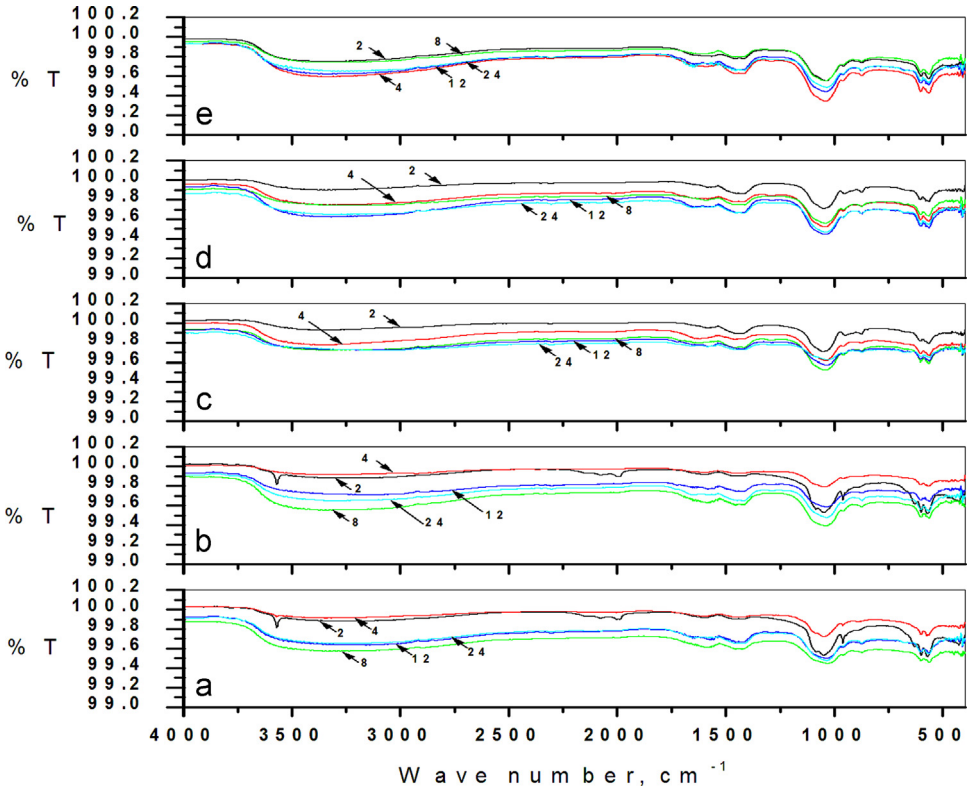

Fig. 11. FTIR spectrum of the surface of the nanocomposite samples as a function of time immersed in SBF for the bioactivity study.

apatite formation when exposed to SBF for up to 24 weeks, with only 1.15% haemolysis. However, there was a compromise between the mechanical properties observed and the in vitro bioactivity studied up to 24 weeks, and care must be taken before selecting any final applications of the nanocomposites.

Acknowledgements

The authors wish to thank the personnel at the Bioceramics and Coating Division and Non-Oxide Ceramics Division, CSIR-CGCRI, Department of Chemical Engineering, Jadavpur University for their generous help and kind support in performing the necessary R&D experiments. We also wish to thank the Council of Scientific and Industrial Research (CSIR) and the University Grants Commission (UGC) for their financial support.

References

[1] S. Iijima, Helical microtubules of graphitic carbon, Nature 354 (6348) (1991) 56–58.
[2] M.-F. Yu, O. Lourie, M.J. Dyer, K. Moloni, T.F. Kelly, R.S. Ruoff, Strength and breaking mechanism of multiwalled carbon nanotubes under tensile load, Science 287 (5453) (2000) 637–640.
[3] J.-P. Salvetat, A.J. Kulik, J.-M. Bonard, G.A.D. Briggs, T. Stöckli, K. Metenier, S. Bonnamy, F. Beguin, N.A. Burnham, L.s. Forró, Elastic modulus of ordered and disordered multiwalled carbon nanotubes, Adv. Mater. 11 (2) (1999) 161–165.
[4] E.W. Wong, P.E. Sheehan, C.M. Lieber, Nanobeam mechanics: elasticity, strength, and toughness of nanorods and nanotubes, Science 277 (5334) (1997) 1971–1975.
[5] R.S. Ruoff, D.C. Lorents, Mechanical and thermal properties of carbon nanotubes, Carbon 33 (7) (1995) 925–930.
[6] F. Lupo, R. Kamalakaran, C. Scheu, N. Grobert, M. Ruhle, Microstructural investigations on zirconium oxide–carbon nanotube composites synthesized by hydrothermal crystallization, Carbon 42 (10) (2004) 1995–1999.
[7] T. Seeger, G. de la Fuente, W.K. Maser, A.M. Benito, M.A. Callejas, M.T. Martínez, Evolution of multiwalled carbon-nanotube/SiO_2 composites via laser treatment, Nanotechnology 14 (2) (2003) 184–187.
[8] R.Z. Le Geros, J.P. Le Geros, Dense hydroxyapatite, in: L.L. Hench, J. Wilson (Eds.), An Introduction to Bioceramics, World Scientific, Singapore, 1993, p. 139.
[9] L.G. Yu, K.A. Khor, H. Li, P. Cheang, Effect of spark plasma sintering on the microstructure and in vitro behavior of plasma sprayed HA coatings, Biomaterials 24 (16) (2003) 2695–2705.
[10] S.K. Nandi, S. Roy, P. Mukherjee, B. Kundu, D.K. De, D. Basu, Orthopaedic applications of bone graft and graft substitutes: a review, Indian J. Med. Res. 132 (7) (2010) 15–30.
[11] J.A. Delgado, L. Morejoń, S. Martinez, M.P. Ginebra, N. Carlsson, E. Fernandez, J.A. Planell, M.T. Clavaguera-Mora, J. Rodriguez-Viejo, Zirconia-toughened hydroxyapatite ceramic obtained by wet sintering, J. Mater. Sci.: Mater. Med. 10 (12) (1999) 715–719.
[12] X. Zhang, G.H.M. Gubbels, R.A. Terpstra, R. Metselaar, Toughening of calcium hydroxyapatite with silver particles, J. Mater. Sci. 32 (1) (1997) 235–243.
[13] M. Zakeri, E. Hasani, M. Tamizifar, Mechanical properties of TiO_2–hydroxyapatite nanostructured coatings on Ti–6Al–4V substrates by APS method, Int. J. Miner.: Metall. Mater. 20 (4) (2013) 397–402.
[14] M.A. Lopes, F.J. Monteiro, J.D. Santos, Glass-reinforced hydroxyapatite composites: fracture toughness and hardness dependence on microstructural characteristics, Biomaterials 20 (21) (1999) 2085–2090.
[15] A. Chanda, S. Dasgupta, S. Bose, A. Bandyopadhyay, Microwave sintering of calcium phosphate ceramics, Mater. Sci. Eng. C 29 (4) (2009) 1144–1149.
[16] Y. Zhang, S. Tan, Y. Yin, C-fibre reinforced hydroxyapatite bioceramics, Ceram. Int. 29 (1) (2003) 113–116.
[17] H. Najafi, Z.A. Nemati, Z. Sadeghian, Inclusion of carbon nanotubes in a hydroxyapatite sol–gel matrix, Ceram. Int. 35 (7) (2009) 2987–2991.
[18] C. Kaya, Electrophoretic deposition of carbon nanotube-reinforced hydroxyapatite bioactive layers on Ti–6Al–4V alloys for biomedical applications, Ceram. Int. 34 (8) (2008) 1843–1847.
[19] Y. Chen, Y.Q. Zhang, T.H. Zhang, C.H. Gan, C.Y. Zheng, G. Yu, Carbon nanotube reinforced hydroxyapatite composite coatings produced through laser surface alloying, Carbon 44 (1) (2006) 37–45.
[20] B. Kundu, M.K. Sinha, M.K. Mitra, D. Basu, Fabrication and characterization of porous hydroxyapatite ocular implant followed by an in vivo study in dogs, Bull. Mater. Sci. 27 (2) (2004) 133–140.
[21] K. Niihara, R. Morena, D.P.H. Hasselman, Evaluation of K_{1c} of brittle solids by the indentation method with low crack-to-indent ratios, J. Mater. Sci. Lett. 1 (1) (1982) 13–16.
[22] W.C. Oliver, G.M. Pharr, An improved technique for determining hardness and elastic modulus using load and displacement sensing indentation experiments, J. Mater. Res. 7 (6) (1992) 1564–1583.
[23] T. Kokubo, H. Kushitani, S. Sakka, T. Kitsugi, T. Yamamuro, Solutions able to reproduce in vivo surface-structure changes in bioactive glass-ceramic A-W3, J. Biomed. Mater. Res. 24 (6) (1990) 721–734.
[24] B.D. Cullity, Element of X-ray Diffraction, 2nd ed., Addison Wesley Pub. Co., Reading, MA, 1978.
[25] D. Basu, B. Mukherjee, Sintering of ceramics, in: S. Kumar (Ed.), Handbook of Ceramics, vol. 2, Kumar and Associates, Kolkata, 1997, pp. 168–181.
[26] L. Niu, H. Kua, D.H.C. Chua, Bonelike apatite formation utilizing carbon nanotubes as template, Langmuir. 26 (6) (2009) 4069–4073.
[27] T.L. Norman, D. Vashishth, D.B. Burr, Fracture toughness of human bone under tension, J. Biomech. 28 (3) (1995) 309–320.
[28] J.M. Hodgkinson, Mechanical Testing of Advanced Fibre Composites, Woodhead Publishing Ltd., Cambridge, 2000.
[29] L.L. Hench, Bioceramics: from concept to clinic, J. Am. Ceram. Soc. 74 (7) (1991) 1487–1510.
[30] J. Chlopek, B. Czajkowska, B. Szaraniec, E. Frackowiak, K. Szostak, F. Beguin, In vitro studies of carbon nanotubes biocompatibility, Carbon 44 (6) (2006) 1106–1111.
[31] P. Galvan-Garcia, E.W. Keefer, F. Yang, M. Zhang, S. Fang, A. A. Zakhidov, R.H. Baughman, M.I. Romero, Robust cell migration and neuronal growth on pristine carbon nanotube sheets and yarns,, J. Biomater. Sci., Polym. Ed. 18 (10) (2007) 1245–1261.
[32] L.P. Zanello, B. Zhao, H. Hu, R.C. Haddon, Bone cell proliferation on carbon nanotubes, Nano Lett. 6 (3) (2006) 562–567.